Cortical networks relating to arousal are differentially coupled to neural activity and hemodynamics

Lisa Meyer-Baese[1,2], Arthur Morrissette[1], Yunmiao Wang[1], Brune Le Chatelier[1], Peter Borden[2], Shella Keilholz[2], Garrett Stanley[2], and Dieter Jaeger[1]

1. Emory University, Department of Biology
2. Dept. of Biomedical Engineering, Emory and Georgia Tech

Contact Author: djaeger@emory.edu

Acknowledgements

We thank Dr. Thomas Knöpfel for sharing the VSFP 1.2 construct along with valuable advice on their use. We thank Dr. Hongkui Zeng for providing the initial VSFP mice for our colony. This work was supported by National Institute of Neurological Disorders and Stroke (UO1NS094302 and R01ns078095), National Institutes of Health BRAIN Initiative (R01 NS111470), and National Institute of Biomedical Imaging and Bioengineering (T32EB025816 and R01eb029857).

Abstract

Even in the absence of specific sensory input or a behavioral task, the brain produces structured patterns of activity. This organized activity has been shown to be modulated by changes in arousal. Here, we use wide-field voltage imaging to establish the relationship between cortical network activity and arousal in spontaneously behaving head-fixed mice expressing the voltage sensitive fluorescent FRET sensor Butterfly 1.2. This approach allowed us to simultaneously image hemodynamic and voltage activity, and then compare fMRI analogous activity changes to the direct cortical voltage activity in relation to arousal and movement. Arousal and facial movements were assessed through analysis of face video recordings. We find that changes in pupil diameter were differentially coupled to hemodynamics and cortical voltage activity in a regionally and frequency specific way. Further this coupling changed between periods of spontaneous facial movements, and periods of rest. Our results indicate that while fMRI-like hemodynamic signals show strong relations to behavior and arousal, these relations are distinct from those shown by brain voltage activity.

Introduction

The cerebral cortex shows constant activity even in the absence of overt behaviors. This spontaneous resting state activity has been used in humans, primates, and rodents to study the functional architecture of the brain (Biswal, Zerrin Yetkin, Haughton, & Hyde, 1995; Fox, Zhang, Snyder, & Raichle, 2008; Meyer-Baese, Watters, & Keilholz, 2022) Distinct synchronization existing between brain regions is interpreted to represent the connectivity of intrinsic functional neural networks. The study of these resting state functional connectivity networks is predominantly done using functional magnetic resonance imaging (fMRI). While resting state fMRI (rsfMRI) has the advantage of getting whole-brain coverage in a noninvasive manner, the measured blood oxygen level-dependent (BOLD) signal only serves a surrogate measurement of neural activity. To relate functional networks characterized with fMRI and neural activity, we need a simultaneous measurement of both extending over multiple cortical areas. The current study achieves this important goal by simultaneously measuring hemodynamic and voltage signals across dorsal cortex of mice.

Spontaneous resting state fluctuations are proposed to encode ongoing behavioral and cognitive variables such as changes in arousal and movement (McGinley et al., 2015; Reimer et al., 2014). Previous studies have validated pupil diameter changes as a measure for arousal both in humans and animal models (Alnaes et al., 2014; DiNuzzo et al., 2019; Murphy, O'Connell, O'Sullivan, Robertson, & Balsters, 2014; Reimer et al., 2016). Animal models have become an important tool for investigating what drives changes in resting-state activity (Pais-Roldán et al., 2021). In rodents a direct relationship is known to exist between increases in arousal and increases in pupil diameter at a short time lag (McGinley et al., 2015; Reimer et al., 2014; Shimaoka, Harris, & Carandini, 2018; Vinck, Batista-Brito, Knoblich, & Cardin, 2015). Animal movement, often measured by periods of locomotion, has also been observed to influence arousal levels. Such locomotion leads to long dilations in pupil diameter and periods of desynchronized cortical activity (McGinley M.; Shimaoka et al., 2018; Vinck et al., 2015). Furthermore, changes in arousal appear to be differentially coupled across different frequency bands which potentially is mediated by fluctuations in activity of noradrenergic and cholinergic projection systems to cortex (Reimer et al., 2016).

In human BOLD-fMRI research pupil-related activations are known to influence cortical areas that regulate selective attention, salience, and decision-making (DiNuzzo et al., 2019). Positive coupling between BOLD and pupil diameter is observed in regions comprising cingulo-opercular, default mode and fronto-parietal networks while negative coupling with visual and sensorimotor regions (Breeden, Siegle, Norr, Gordon, & Vaidya, 2017; DiNuzzo et al., 2019). To what degree resting-state networks assessed with fMRI reflect electrical neuronal population activity, and whether electrical activity shows the same relationship to behavioral and cognitive variables as hemodynamics is not well understood.

In this work we sought to examine the detailed relationship between neuronal population activity and hemodynamics with respect to arousal and spontaneous movement in waking mice. To this end, we used wide-field voltage imaging in voltage-sensitive fluorescent protein (VSFP) expressing mice using the Butterfly 1.2 sensor (Akemann et al., 2012). Crossing cre-dependent Butterfly 1.2 mice with an EMX1 cre strain, we were able to measure changes in neural activity in excitatory neurons and hemodynamics across dorsal cortex. We simultaneously monitored changes in pupil diameter and orofacial movements to enable us to parse the spatial and temporal contributions of both arousal and orofacial motion on cortical activity.

Our results show similarities as well as important differences in the correlation of arousal with neuronal population voltage activity and the hemodynamic signal. Further, the spatial activity correlation maps with arousal depended differentially on the behavioral state of the animal in a signal frequency dependent manner. Our results indicate that arousal related brain networks are dynamically regulated, and only partly overlap between functional networks determined from hemodynamic or voltage activity.

Materials and Methods

Animal model

Mice expressing the VSFP-Butterfly 1.2 in excitatory neurons in all layers of cortex were bred at Emory University. To do so, Camk2a-tTA;Ai78(TITL-VSFPB) double-cross Tg mice were obtained from Dr. Hongkui Zeng. These mice were further crossed with a homozygous Emx1-cre line expressing cre in excitatory neurons across all cortical layers (Jax 005628). Triple positive mice robustly express VSFP Butterfly 1.2 fluorescence throughout the cell bodies and neuropil of excitatory neurons in the entire cerebral cortex (Figure 1). Note that VSFP mice can also be derived from first crossing the cre/tTa dependent VSFP-Butterfly reporter line (Madisen et al., 2015) (Ai78-Jax 023528) with a CamK2a-tTa line expressing tTa in excitatory neurons (Jax 007004), followed by a cross with the EMX1 cre-line.

Voltage imaging

For voltage imaging of excitatory neurons, mice (n=5) were prepared with a clear-skull window as previously described (Silasi, Xiao, Vanni, Chen, & Murphy, 2016). The cranial window consisted of a custom-cut glass coverslip cemented over the cleaned skull surface. A thin layer of cyanoacrylate glue was placed in between the bone and cement interface. Mice were administered 0.1mg/kg of buprenorphine SR as a long lasting analgesic before starting the surgery, and anesthetized with 1-2% isoflurane (3-4% for induction). All experimental procedures were approved by the Emory University Institutional Animal Care and Use Committee.

VSFP signals were imaged from awake, head-fixed mice, using a macroscope (MiCAM Ultima, Brainvision Inc.) based on the tandem lens and epi-illumination system design (Ratzlaff & Grinvald, 1991). The imaging plane of the macroscope was focused through the intact skull slightly below (~100μm) the most superficial blood vessels. Excitation light was provided by a blue LED (LEX2-B, Brainvision Inc.), through a band-pass filter at 482nm (FF01-482/35, Semrock Inc.) and a dichroic mirror (FF506-Di03, Semrock Inc.). VSFP-Butterfly FRET is a unimolecular sensor that contains two different-colored chromophores which act as the FRET donor (mCitirine) and acceptor (mKate2). The emission of mCitirine and mKate2 was imaged through two CMOS cameras (MiCAM-Ultima). The first camera recorded the emitted green fluorescence from mCitrine, which was reflected by a second dichroic mirror (FF593-Di03, Semrock, Inc.) and passed through an emission filter (FF01-543-50-25, Semrock Inc.). The second camera recorded the emitted red fluorescence from mKate2, passed through the second dichroic mirror and an emission filter (BLP01-594R-25, Semrock Inc.). The camera acquisition was controlled by the MiCAM Acquisition Software. Acquisition frame rates varied between 25-200Hz with a spatial resolution of 100x100μm per pixel for a 100x100 pixel array.

An additional camera was set-up to monitor and record changes in behavioral state and pupil diameter. This was done by acquiring a 10-25Hz video of the side of the mouse face during each imaging session. The camera was positioned for capturing the left side of the mouse face as well as the left eye and the area where the forelimbs often rest underneath the mouse body.

All 5 animals were imaged during multiple imaging sessions for multiple trials (n = 65 trials in total) where each imaging trial ranged from 20 to 160 seconds.

Cortical local field potential (LFP) recording in conjunction with VSFP imaging in lightly anesthetized mice

LFP activity was recorded from barrel cortex in lightly anesthetized mice. Animals underwent surgery for the cranial window and a head-bar implant at least a week prior to the recording. At the day of LFP recording, the animals were first put under 2% isoflurane anesthesia for drilling a craniotomy. The glass cover and dental cement above barrel cortex were carefully removed using a dental drill. After the skull was successfully exposed, a small craniotomy with the size of 1 x 2 mm was drilled by the edge of the imaging window. The exposed dura was then covered with a thin layer of Dura Gel (Cambridge Neurotech). For data collection, animals were transferred and head-fixed under the imaging setup. The isoflurane level was lowered to 1%, and the temperature of a heating pad below the mouse was maintained at 37°. A 32-Channel silicon probe with sharpened tip (Part H7b from Cambridge Neurotech) was slowly lowered into the craniotomy at a 45-degree angle to a depth of around 900µm. Acute LFP data were recorded via an RHD USB interface board (Intan Technologies) at 20 kHz. For LFP analyses, the signals across all 32 channels were band-pass filtered between 0.01 and 50 Hz.

VSFP image processing

Raw images from both the donor and acceptor cameras were first aligned and registered to the first frame of the green channel for any given trial to perform within trial image registration. The red and green fluorescence signals from the two cameras were analyzed to extract the voltage and hemodynamic signals using the gain-equalization method as previously described (Akemann et al., 2012; Carandini et al., 2015; Shimaoka et al., 2018). The gains at the heartbeat frequency were equalized between the two cameras. The gain equalization factors were obtained once per recording for each pixel, using the first trial of the session. The ratio of the two cameras captures FRET signals linked to membrane voltage variations (Carandini et al., 2015) while the sum of the two signals captures large co-fluctuations linked to the hemodynamic response (Shimaoka et al., 2018). To exclude possible residual contamination of the hemodynamics in the ratiometric voltage signal, the sum (hemodynamic) signal was filtered below 5Hz and then scaled by the regression coefficient with the ratiometric signal, then regressed out from the ratiometric voltage signal (hemodynamic signal regression).

To perform analyses across trials and mice, the base image used to register within-trial frames was aligned to a template cortical map derived from the Allen Brain Mouse Atlas v3 (brain-map.org). A 2D top projection of the annotated Allen Brain Atlas volume was created in MATLAB (MathWorks) and a template image from each mouse was registered to the atlas using an affine transformation computed from two control points that were selected manually: the mid-point at the top of the front portion of dorsal cortex and the base of the cortex at the midline of the retrosplenial cortex. Once all frames were aligned, a mask of the 2D Allen Atlas was created in MATLAB and applied which set all pixels outside of cortex to zero.

Pupil diameter

To determine the pupil diameter, video frames showcasing the side of the mouse face were first cropped to include only the eye. Pupil diameter was often acquired through the whisker field with whisker motion in front of the pupil limiting the use of existing methods for determining pupil diameter (Reimer et al., 2014; Stringer et al., 2019). A fast pupil detection method using custom-made Matlab scripts was

developed to determine diameter of the pupil frame-by-frame. First, the pixel intensity threshold was set through an interactive user interface to binarize the darkest regions representing the pupil; then the edges of the pupil (which may be composed of multiple objects if whiskers obstruct continuous object isolation) were determined and the distances between all of the edge points was used to calculate the maximum projection across the object(s) representing the pupil diameter. This method is both fast and robust to objects crossing the pupil and creating discontinuities in the ellipse shape of the pupil. Lastly, the pupil diameter trace was smoothed with a 10th order median filter. This removed artifacts such as a portion of the whiskers occluding the pupil across 1-2 frames during diameter detection.

Orofacial movements

Periods of movement and quiescence were estimated from video capturing the side of the mouse face including: snout, whiskers, and jaw. The onset and offset of movement periods were detected based on average changes in pixel intensity between frames. Orofacial movement signals of each pixel were differentiated and squared. Periods when the frame movement was 2SD above the motion estimate were classified as periods of orofacial movement. Across a single trial, movement periods were classified as points in time where the orofacial movement signal remained above threshold for at least 2 seconds. Rest periods where those periods in which the movement signal remained below threshold for at least 2 seconds.

Frequency analysis

The time varying power of different frequencies was calculated for all signals using wavelet spectrograms with the Morlet Wavelet. To assess coherence between different pairs of signals we used the built in MATLAB function wcoherence() again using the Morlet Wavelet. The obtained scalograms are susceptible to edge-effect artifacts. These arise from areas where the stretched wavelets extend beyond the edges of the observation interval. Only information within the unshaded region delineated by the white line presents an accurate time-frequency representation of the data. Therefore, all trial averaged data was obtained by disregarding the data outside of these bounds. For cross-trial comparisons the magnitude squared coherence values for each single trial was calculated and averaged across trials as a function of frequency. Plots show the mean magnitude squared coherence value, within an ROI or across the whole brain, with error bars representing the standard error.

Cross-correlation

Unless otherwise indicated all correlation values represent the maximum correlation value obtained from calculating the cross-correlation between two discrete-time sequences using the built in matlab function [r,lag] = xcorr(x,y). The cross-correlation measures the similarity between vector x, which is always either the voltage or hemodynamic signal, and shifted (lagged) versions of vector y which in all cases represents the pupil diameter.

Global Signal

For whole brain analysis, the global signal was used for both voltage and hemodynamic signals. Global signal represents a timeseries of signal intensity averaged across all pixels in cortex. For each animal and imaging session, global voltage and hemodynamic traces were obtained by averaging the z-scored signal from each pixel located within cortex while masking pixels outside. Z-scored signals were used to ensure each pixel contributed equally to the calculation of global signal and that local transients of activity (either noise or physiological) did not bias the global signal calculation.

ROIs

For ROI specific analysis the signals represent the local averaged signal that represents the shared dynamics of the defined region. ROIs were manually selected once for each animal based on specific areas that show clear signals in the obtained average pupil - voltage activity cross-correlation coefficient map.

Significance testing

Statistical significance between correlation maps was calculated using Mann-Whitney U-tests which were further Bonferroni corrected to calculate adjusted p-values. Since statistical comparisons were calculated for the extent of the imaging area (10,000 pixels), in order to guarantee a global error probability at a given threshold (0.05, 0.01, etc.) the significance level for a single test (pixel) was obtained by dividing the global error probability by the number of independent tests. For example, if the p-value was initially significant at $p<0.05$, the p-value corrected for multiple comparisons would be $p<0.05/10000$ or $p<0.000005$.

Shuffled controls

Correlation maps were tested against chance correlations by randomly selecting the pupil data series along with the voltage and hemodynamic signals for a total of 100 times. Correlation coefficients were calculated on the shuffled data. The original data was then tested against the shuffled data using Mann-Whitney U-tests.

The coherence was also tested against chance by similarly randomly selecting a pupil trace, a global voltage trace and a global hemodynamic trace. The magnitude squared coherence for 100 of these new signal pairs was calculated and compared against the original data.

Code and data availability

All code used for analysis will be made available on our GitHub upon publication. The imaging data presented here will be published on DANDI (https://dandiarchive.org/) in Neural Data Without Borders (NWB) format (https://www.nwb.org/).

Results

Wide-Field cortical imaging of voltage activity across dorsal cortex

We used wide-field voltage cortical voltage imaging to record from excitatory neural populations primarily in layer 2/3 over the dorsal surface of the brain during spontaneous behavior in head-fixed mice (see Methods). The VSFP Butterfly protein in transgenic animals was expressed throughout the cortex (Fig. 1A) as previously observed (Carandini et al., 2015; Ferezou et al., 2007; Madisen et al., 2015; Ratzlaff & Grinvald, 1991). Wide-field optical signals are very sensitive to physiological variables such as blood flow, blood oxygenation, and intrinsic autofluorescence (Ma et al., 2016; Pisauro, Benucci, & Carandini, 2016). A ratiometric equalization technique (Carandini et al., 2015) was used to compare the two combined fluorescent signals from both the acceptor and donor channel of VSFP Butterfly to estimate average local membrane voltages separately from the hemodynamic signals (Fig 1B). Video of the face was recorded to track changes in orofacial movements and pupil diameter (Fig 1C).

To determine the relationship between voltage imaging signals and electrophysiological voltage activity across cortical layers, laminar LFP recordings were obtained simultaneously with voltage imaging. The

electrode tip was placed to span multiple layers in the barrel cortex in lightly anesthetized mice (n = 2, Fig. 1D). LFP waveforms showed a clear similarity with voltage imaging traces from adjacent areas of cortex (Fig. 1D). We found barrel cortex LFP was also strongly coupled to voltage imaging traces in contralateral barrel cortex as well as ipsilateral and contralateral motor cortex with a maximum correlation of 0.5 (Fig. 1E), revealing a sensorimotor network of co-activity under light isoflurane anesthesia. These findings indicate a clear relationship between LFP activity and layer 2/3 voltage imaging, though voltage imaging is showing signal averages across 0.1 x 0.1 mm areas of cortex, and contributions from deeper layers likely differ between the two methods.

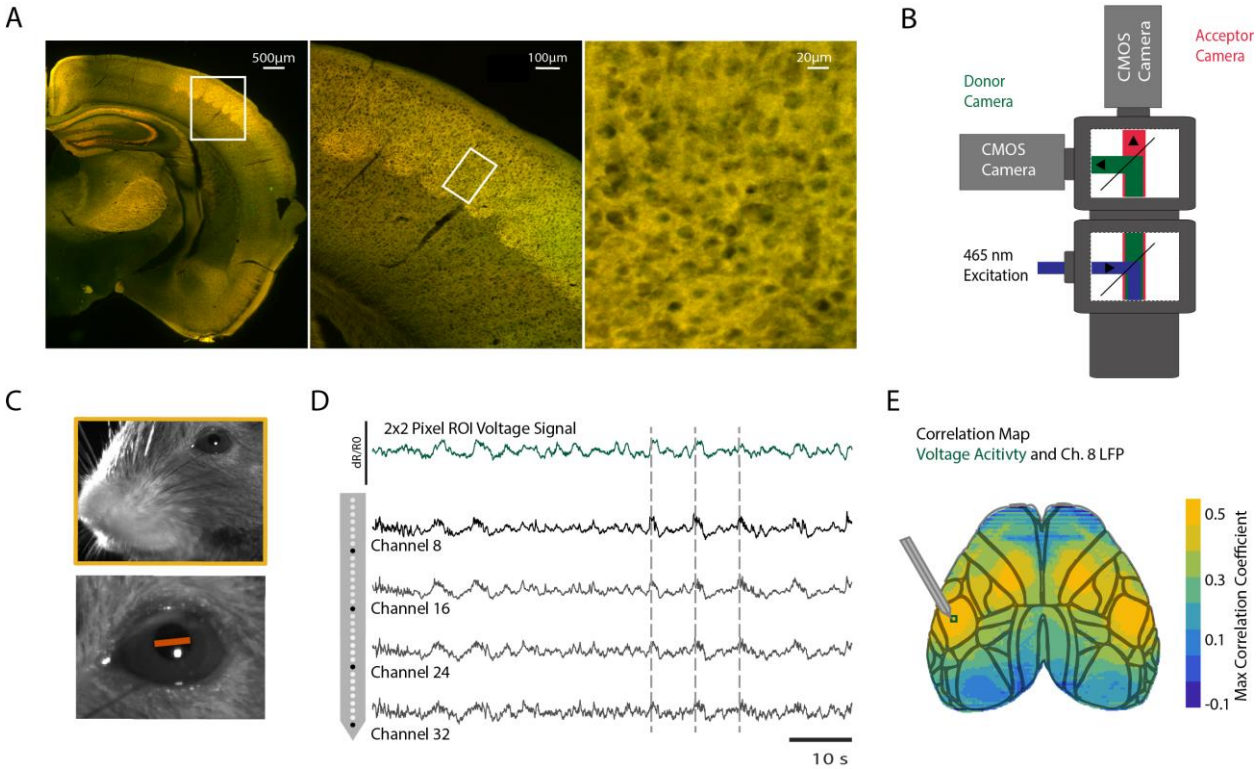

Figure 1 Expression and validation of genetically encoded VSFP protein A. A coronal section of one hemisphere at bregma -1.5 mm depicting combined red and green fluorescence channels reveals cortical VSFP Butterfly 1.2 expression across dorsal cortex. Barrel cortex (white box in left panel) is expanded in resolution to show the membrane associated expression of Butterfly 1.2. Note that voltage imaging is not dependent on even expression of VSFP 1.2 across areas since local ratiometric signals are evaluated. **B.** Imaging set-up to record voltage activity across wide extents of dorsal cortex, using an epi-illumination macroscope containing a 465nm excitation LED and two cameras to capture fluorescent light for both green and red wavelengths, which corresponds to the donor and acceptor fluorophores of the FRET based VSFP-Butterfly 1.2 sensor. **C.** The top image shows an example frame from video acquisition of the mouse face during cortical imaging. The region of interest used for analysis of spontaneous facial movements is depicted by the surrounding yellow box. Visible areas of the mouse face contributing to movement signal include the nose, snout, jaw, and whiskers of the mouse. The bottom image shows the cropped region of interest for calculating the pupil diameter during cortical imaging. The red line represents the maximum width across the pupil used as the measure of pupil diameter. **D.** Comparing cortical voltage activity and laminar LFP analysis in anesthetized mouse. The top trace (green) shows the average voltage signal from a 2-by-2-pixel ROI next to the LFP electrode as shown to the right on the cortical map (green square). The 4 signal traces below correspond to the positioning of 4 channels on the laminar probe, which was inserted at an angle of 45 degrees into the left barrel cortex. **E.** The average correlation map shows the correlation between voltage activity in the ROI close to the LFP electrode and the channel 8 LFP signal. More widely, barrel cortex and an area more anterior in the motor cortex are highly correlated with the LFP trace.

Pupil diameter is tightly coupled to global cortical signal changes in voltage but not hemodynamics

First, we were interested to determine whether cortical signal changes might globally fluctuate with arousal as measured by pupil diameter. When plotting the global voltage signal and pupil diameter

activity together, a strong similarity in the resulting waveform is readily apparent (Fig. 2A), with a possible delay between voltage and pupil signal. To quantify and examine the variability of time lag between the pupil diameter and the global voltage, a cross-correlation between the global signal and the pupil diameter was calculated (see Methods). A lag was not observed when data from all mice were averaged. What remained consistent, however, was the strong correlation between the two signals with a peak correlation of ~0.5 (Fig2C). These results indicate a strong relation between average cortical activation and arousal as measured by pupil diameter. Previous work imaging noradrenergic and cholinergic axons in layer 1 of visual cortex showed a delay of 0.5-1 s between activation of these arousal-related neuromodulatory systems and pupil diameter in rats (Reimer et al., 2016), suggesting that global cortical depolarization increases we observed have a similar lag to neuromodulation, given that our lag with relation to pupil diameter was close to zero.

Global changes in hemodynamic activity were far less correlated to changes in pupil diameter than global voltage was. The peak correlation between hemodynamics and pupil diameter was determined by fixing each trace of global hemodynamics and shifting the pupil trace (Fig 2D). When shifted traces yielding maximal peak correlations were averaged, an inverse relationship between hemodynamics and pupil diameter with a maximum correlation of -0.069 ± 0.053 which was obtained when pupil was shifted by 1.3 seconds to the right. Therefore, global hemodynamic changes were on average observed 1.3 seconds after changes in pupil diameter. Recent work looking at the relationship between changes in total hemoglobin (HbT) and pupil diameter in somatosensory areas for awake mice found a peak correlation of -0.37 ± 0.25 with a delay of 1.3 seconds (Turner, Gheres, Proctor, & Drew, 2020).

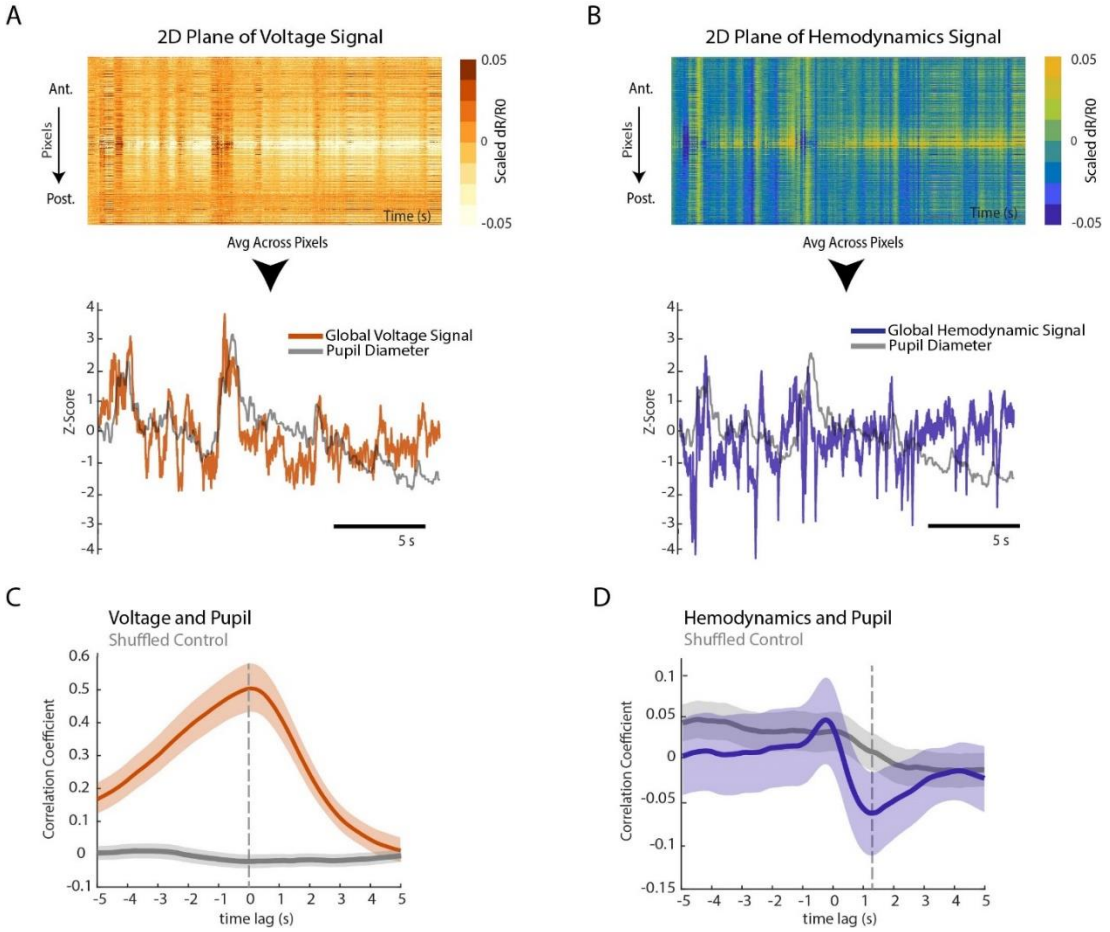

Figure 2 **Coupling of global cortical voltage and hemodynamic signals to changes in pupil diameter A.** All pixels from the cortical surface are laid out in a 2D plane such that the changes in voltage activity for each pixel (y-axis) is represented as a function of time (x-axis). The global signal is obtained by taking the z-score of each pixel and averaging across all pixels. The global voltage signal (yellow) fluctuates in a similar manner to pupil diameter (grey). **B.** Same as in panel A but for cortical hemodynamics signal. A relationship between changes in pupil diameter (grey) and subsequent changes in global hemodynamics (blue) can be observed. Correlation between pupil diameter and global signal is consistent across trials and animals. Where shaded area represents the standard error. **C.** Average cross-correlation between voltage and pupil diameter results in a high correlation of 0.5 centered at ~0s. **D.** Average cross-correlation between hemodynamics and pupil diameter shows an inverse relationship. With max correlation of -0.069 is observed with a delay of 1.3 seconds. Panels C- D show average across n=65 trials for 5 mice. Shaded area represents standard error. Grey trace indicates shuffled control.

Cortical activity and pupil diameter are differentially coupled across functional cortical areas

Our data analysis so far supports a link between changes in arousal as measured by pupil diameter and changes in global cortical voltage signal. To probe for a differential contribution of different cortical areas on the observed correlations, we calculated correlation maps between pupil diameter and changes in cortical voltage and hemodynamics signal at each pixel. Spanning dorsal cortex, we found 4 specific ROIs that displayed a distinct relationship between voltage and arousal bilaterally (Fig 3A,3B). We found that the maximum correlation coefficients between voltage and pupil diameter were highest around medial somatosensory and secondary somatosensory and auditory cortex (Fig 3C, max correlation 0.6). Voltage activity of medial aspects of frontal cortex corresponding to parts of secondary motor and anterior cingulate cortex was also strongly coupled with pupil diameter (Fig3C ROIs 1,3 and 4). In contrast, there was on average zero correlation between pupil diameter and voltage signal in more lateral areas of motor cortex (Fig3C, ROI 2). Overall, however, positive correlations predominated, explaining the positive correlation of global voltage signal with pupil diameter. To assess the statistical significance of observed correlations with voltage, we compared average correlation maps across all trials (n = 65) to a shuffled control (n =100), where voltage traces and pupil diameter traces were taken from different trials. This analysis revealed a significant correlation between voltage activity and pupil diameter for ROIs 1,3 and 4 (Fig. 3D). The net zero correlation that was observed in ROI 2.

We observed a much weaker relationship between pupil diameter and global hemodynamics. However, it is possible that different opposite relations between pupil diameter and hemodynamics in different areas could cancel out. Like voltage, hemodynamics also showed a significant positive correlation with pupil diameter in barrel cortex and more medial somatosensory areas (Fig 3E). The maximal correlation coefficient was lower with 0.2 as opposed to 0.6 for voltage, however. Hemodynamic activity in contrast showed larger and stronger negative maximal correlation peaks than voltage with pupil diameter in frontal medial cortex (Fig 3F, blue areas). We assessed the statistical significance of observed correlations with hemodynamics, using a shuffled control (n =100), where hemodynamic traces and pupil diameter traces were taken from different trials. This analysis revealed a significant correlation between hemodynamic activity and pupil diameter for all 4 ROIs, with ROI 1 and 3 being positively different and ROI 2 and 4 negatively different (Fig 3F). We plotted the cross-correlation function for each ROI to determine the detailed time relationship between pupil diameter changes compared to voltage or hemodynamic activity changes (Fig S3A,B). We found that all positive correlations had their peak with a delay near zero, indicating no average time shift between voltage, hemodynamics, and pupil diameter changes. In contrast, negative correlations between hemodynamics and pupil diameter had a peak correlation at a delay of about 1s, indicating that increases in pupil diameter preceded decreases in hemodynamic activity in these ROIs.

Overall, voltage correlation with pupil diameter showed widespread significant positive correlations including medial prefrontal areas, whereas hemodynamics showed a negative correlation in the same frontal network while maintaining positive correlations in more posterior areas.

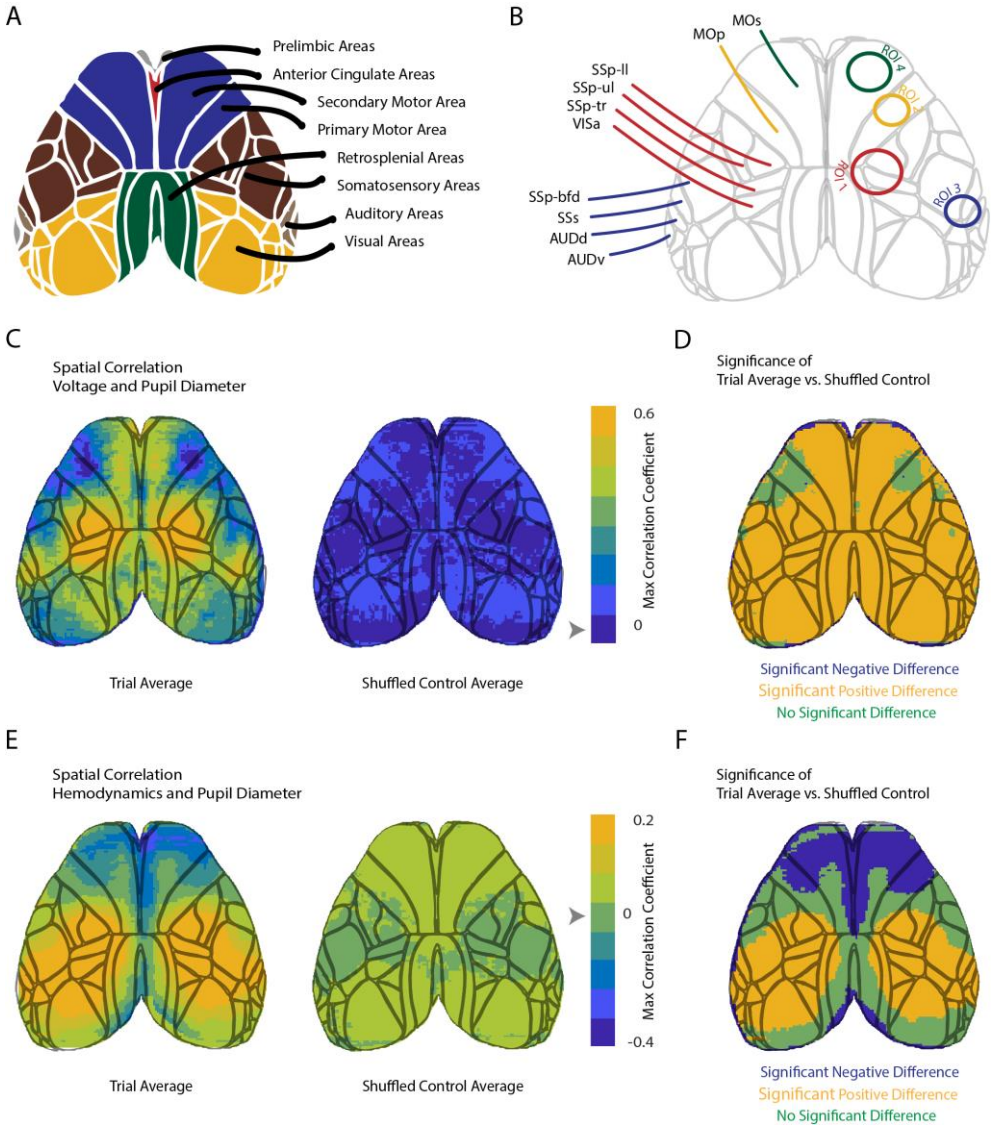

Figure 3 **Region dependent coupling of pupil diameter to voltage and hemodynamic activity across functional cortical areas**

A. Cortical map derived from the Allen Brain Mouse Atlas v3 **B.** Four ROIs that contained regional differences, used in subsequent analysis. **C.** The panel on left represents the average correlation map obtained from all 5 animals (n = 65 trials) between voltage traces and pupil diameter. Strong correlations between voltage activity and pupil diameter above 0.6 which can be observed within the medial sensory-motor cortical areas as well as more laterally in the secondary sensory/ auditory cortices (ROI 1 and 3). There exists also a slight negative correlation with pupil diameter in the more lateral areas of motor cortex (ROI 2). The panel on the right represents the correlation map obtained between 100 randomly selected imaging trials and 100 randomly selected pupil video files. There are no areas that are strongly correlated by chance. **D.** This map shows the significantly different areas between the trial average map and the shuffled control at $p < 0.05$ adjusted for multiple comparisons with Bonferroni Correction (BF). Blue and Yellow represent areas that have a significant negative and positive difference to the control respectively, while green is areas with no significant difference. The map highlights significance across most areas, including ROIs 1,3 and 4. ROI 2 which corresponds to the more lateral area of motor cortex was not statistically different when comparing to the average map. **E.** Panel on the left shows the average coupling between hemodynamic signal and pupil from cross-correlations shows similar positive correlations as seen in voltage activity (ROI 1 and 3). Most notably however is the reduction in correlation, now with a peak slightly above 0.3 as well as the stronger negative correlation of -0.4 that spans primary and secondary motor areas (ROI 2 and 4). Right shows the same as panel C but for hemodynamics. **F.** Same as in panel D but for the relationship between the average trial hemodynamics map and the shuffled control.

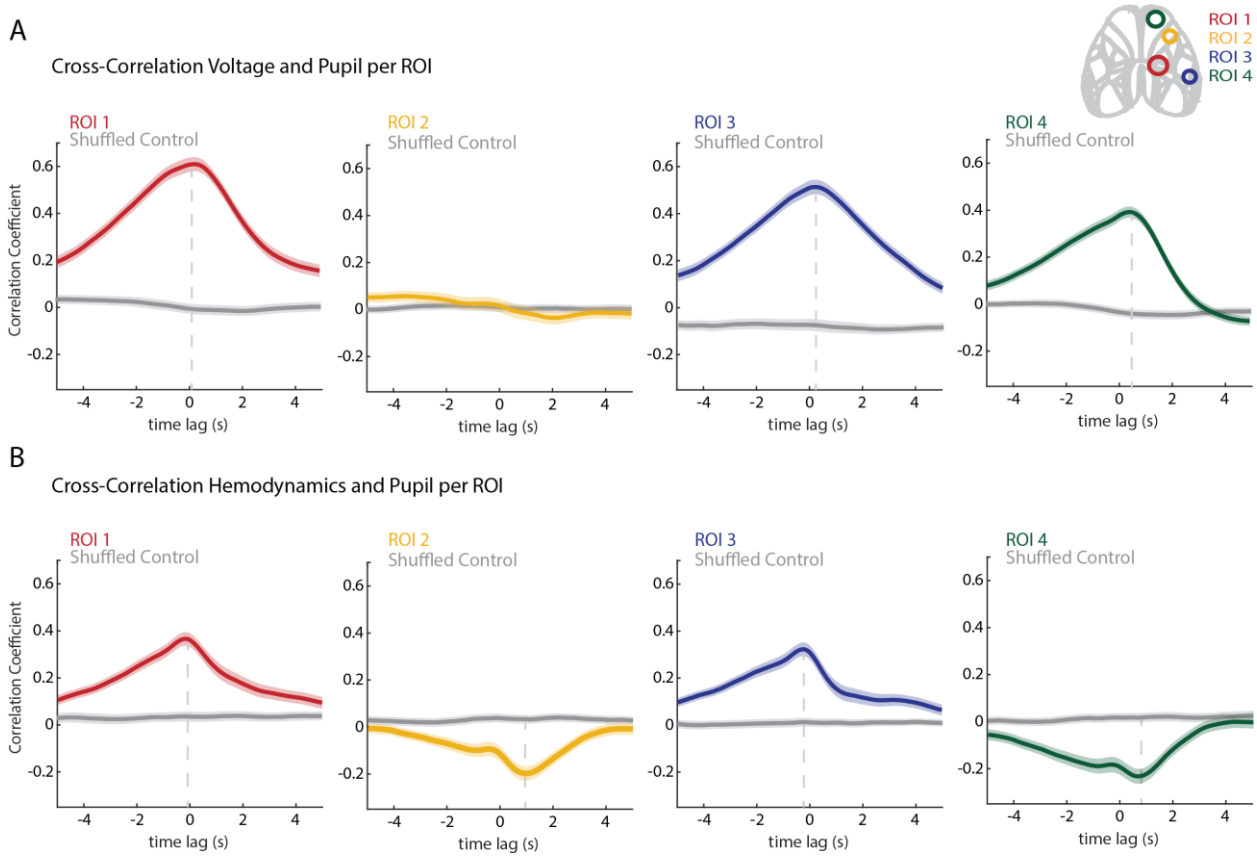

Figure 3 Supplement 1 **Region-dependent cross-correlation of pupil diameter to voltage and hemodynamic activity A.** Average cross-correlation between voltage and pupil diameter per ROI shows region dependent coupling. **B.** Same as in panel A but for hemodynamics and pupil diameter. Note the difference in response for ROI 4 and the different lags for negative peaks. Grey lines indicate shuffled control and shaded area represents the standard error.

Low frequency dependence for pupil diameter, cortical activity, and neurovascular coupling

Next, we sought to determine whether the observed correlations depend on coupling at specific signal frequencies. Visual inspection of both voltage and hemodynamic signals from an ROI in relation to changes in pupil diameter suggests that the observed coupling was driven by slow frequency components present in each of the signals (Fig 4A and 4C, Fig 4SA, SC). Power spectra for voltage, hemodynamics, and pupil diameter all showed higher power at low frequencies (Fig 4B and Fig 4SB,SD). A distinct increase in power between ~8 and 13 Hz was seen only for the hemodynamic signal. This range coincides with the heartbeat frequency of awake mice and is almost certainly reflects the hemodynamic change related to heartbeat.

We further analyzed frequency dependence of voltage and hemodynamic activity related to arousal using wavelet coherence analysis. When looking at voltage and pupil, these two signals were most coherent in the low frequency bands below 0.25Hz for ROIs 1,3 and 4 (Fig. 4D), while ROI 2 that showed a zero-overall correlation between voltage and pupil (Fig. 3C) exhibited the least coherence. The three ROIs where voltage positively correlated with pupil diameter showed very similar coherence with a peak magnitude squared coherence of ~0.8 just below 0.1 Hz. Hemodynamics showed a similar frequency relationship to pupil diameter as voltage, though the peak below 0.1 Hz was smaller with a peak ~0.6, while the coherence between 0.2 and 0.6 Hz was of similar amplitude of 0.4. Higher frequencies not plotted showed no significant coherence when compared to the shuffled control (Fig 4D and E). Coherograms between voltage and hemodynamics (Fig. 4F), showed a peak at low frequencies centered around 0.2 Hz. In addition, voltage and hemodynamics showed a plateau of strong

coherence between ~1.5 to ~6 Hz (Fig. 4F). A shuffle control (Fig. 4 D-F, grey lines) showed no such coherence and indicated that the coherence between voltage and hemodynamics was highly significant up to 9 Hz. This finding indicates that voltage and hemodynamics share higher frequency dynamics that are not related to pupil diameter changes.

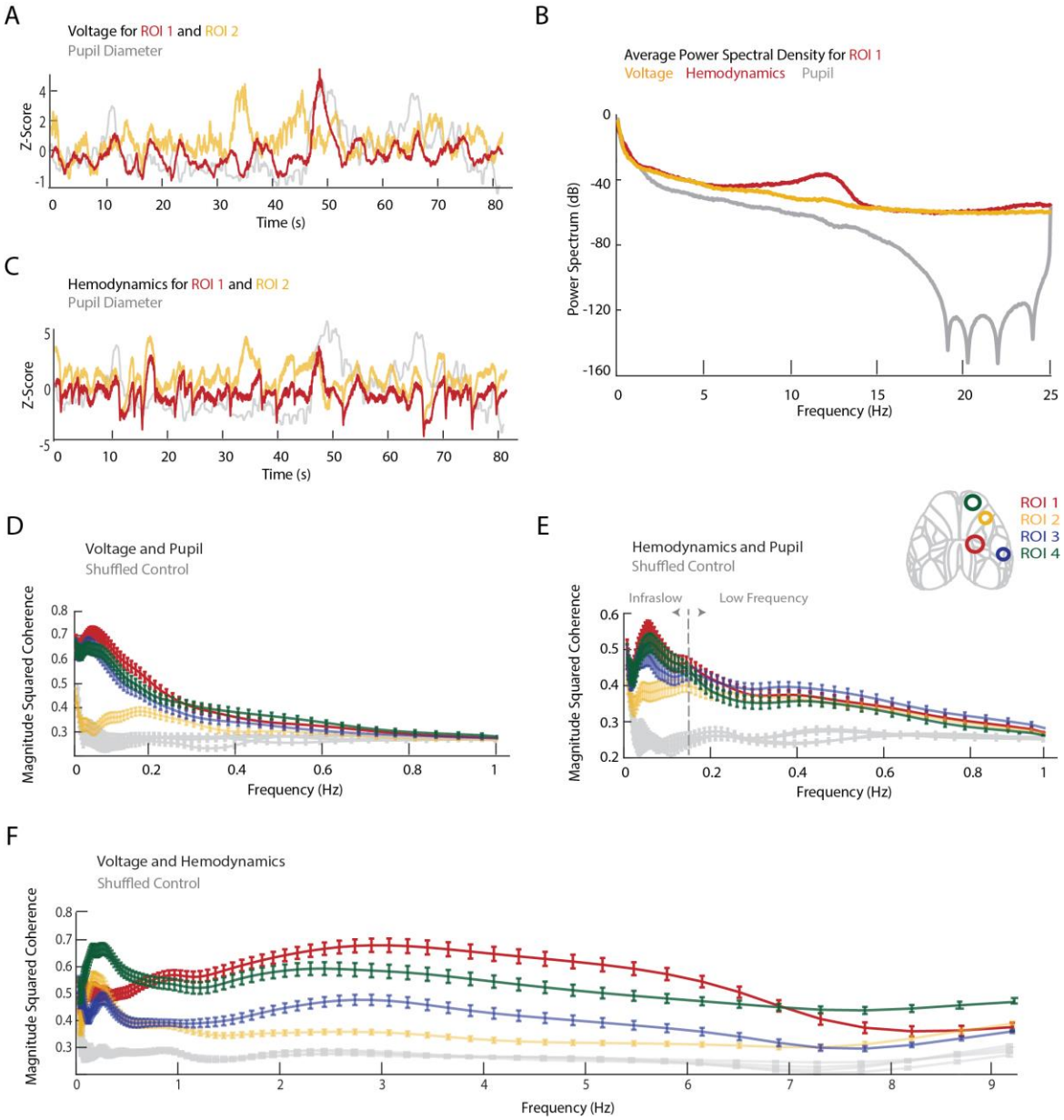

Figure 4 **Region dependent frequency coupling of pupil diameter to voltage and hemodynamic activity A.** Example traces from one trial of voltage activity from ROI 1 and ROI 2. Changes in pupil diameter (grey) are overlaid for reference. **B**. Average power spectral density plot for activity in ROI 1, shown for voltage, hemodynamics and pupil diameter signals (n = 65 trials). **C.** Same as in A but for hemodynamics activity. **D.** Plot shows the average magnitude squared coherence for all trials for pupil and voltage within the cone of influence. **E.** Average magnitude squared coherence for all trials for pupil and hemodynamics within the cone of influence. Each line represents the average values from each ROI with the bars indicating the standard error. Allen Atlas is for referencing ROI location. **F.** The magnitude squared coherence between hemodynamics and voltage across all trials (n = 65) within the cone of influence. Each line represents the average values from each ROI with bars indicating the standard error. For panels D, E and F each line represents the average values from each ROI with the bars indicating the standard error (n = 65 trials, 5 mice). Due to edge effects, less credence is given

to areas of apparent high coherence that are outside or overlap with the cone of influence. Plots therefore disregard the first and last 20 seconds. The 4 grey lines for panel D-F represent the average magnitude coherence (n = 100) obtained by comparing a randomly selected hemodynamic traces with a randomly selected voltage trace from different trials for each ROI. The error bars represent standard error.

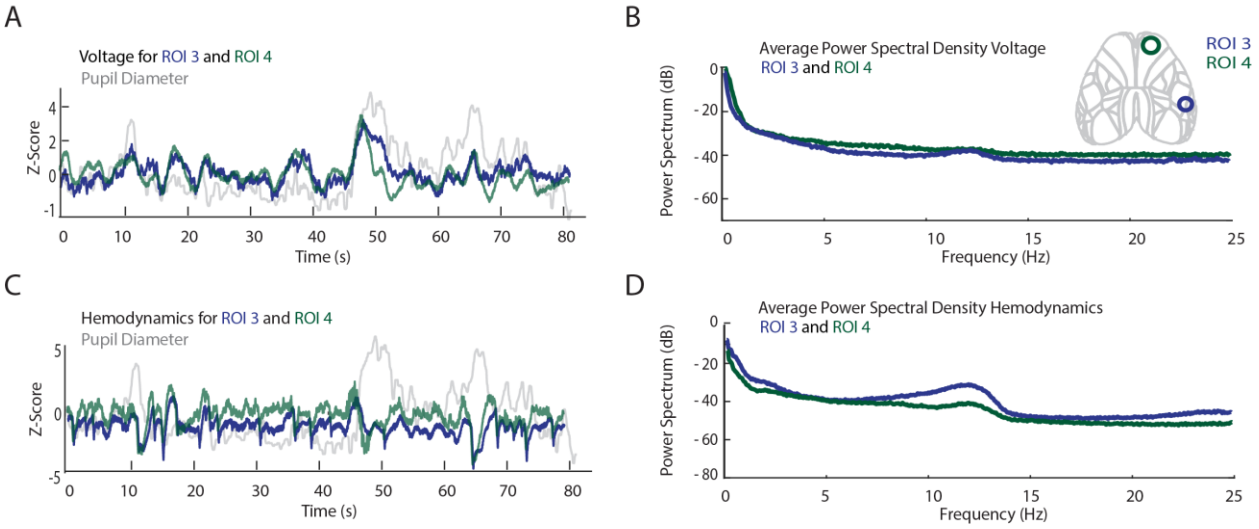

Figure 4 Supplement 1 **A.** Example voltage traces from same trial as in Figure 4, panel A but now shown for ROI 3 and 4. **B. Average** power spectrum for voltage activity in ROI 3 and 4 (n = 65 trials). **C.** Same as in A but for hemodynamics. **D.** Same as in B but for hemodynamics.

Patterns of cortical coupling to pupil diameter are dependent on behavioral state

Previous studies have described large effects of behavioral state on membrane voltage across multiple brain regions (Ferezou et al., 2007; Poulet & Petersen, 2008; Shimaoka et al., 2018). To characterize the effects of behavioral state on the coupling between cortical voltage and hemodynamic activity and pupil diameter, we separated cortical activity between periods of movement and rest. Movement periods were determined from a video of the face as periods of spontaneous orofacial movements. These orofacial movements consisted of changes in whisker, jaw, or snout position (see Methods), and occurred in distinct bouts (Fig. 5A). Pronounced pupil diameter changes were frequently associated with periods of movement, whereas such changes were more modest in the absence of movement (Fig. 5A).

The data was further split into two frequency bands, a low passed (LP) infraslow signal <0.15Hz and a band passed (BP) 0.15 – 1 Hz (Fig 4E) slow activity signal. These two frequency bands displayed distinct coherence with pupil diameter (Fig. 4D,E) and are also within the range of frequencies that can be resolved with fMRI.

Our analysis revealed substantial differences between cortical voltage and hemodynamic activity coupling to pupil diameter dependent on the presence of spontaneous movements. When animals were resting, correlations between pupil and voltage or hemodynamic activity were near-absent below 0.15 Hz (Fig. 5B, left panels). This observation may at least in part due the relative lack of pupil diameter changes during these periods.

In the presence of facial movement, large areas of cortex showed correlations between voltage and pupil diameter below 0.15 Hz, while the correlations between hemodynamics and pupil diameter were much

more restricted to medial somatosensory and motor areas (Fig. 5B, right panels). Statistical comparison between rest and movement periods compared to a shuffled control revealed a significant influence of medial sensory areas during both behavioral states for voltage, with movement periods driving also significant correlations in prefrontal and anterior spanning sensory, visual, and auditory cortices (Fig 5C, top panels). In comparison hemodynamic signal correlations were only significant during movement, with strong positive changes observed in medial sensory cortex and strong negative changes in prefrontal cortex (Fig 5C, bottom panels).

Cortical activity signals at frequencies between 0.15 and 1 Hz showed a substantially different relationship with orofacial movements than the infraslow signal. Here, a pronounced widespread correlation was found between hemodynamics and pupil diameter at rest (Fig. 5D, bottom left), which was largely absent during movement (Fig. 5D, bottom right). A relation between voltage and pupil diameter was also present in this frequency band, but this was spatially limited to barrel cortex (Fig. 5D and 5E, top left). Interestingly, during movement periods, this relationship disappeared in barrel cortex, but instead a different area more medially now correlated strongly with pupil diameter (Fig. 5D and 5E, top right). These findings indicate the presence of two distinct functional relations between pupil diameter and cortical voltage activity between periods of rest and periods of spontaneous facial movements. In contrast hemodynamic activity was more exclusively and globally related to pupil diameter at rest, and only weekly during movement.

Overall, these data reveal a clear dissociation between how the hemodynamic signal relates to pupil diameter in comparison to brain voltage activity. Further, the relationship for both signals is distinctly different for infraslow frequencies than frequencies between 0.15 and 1 Hz.

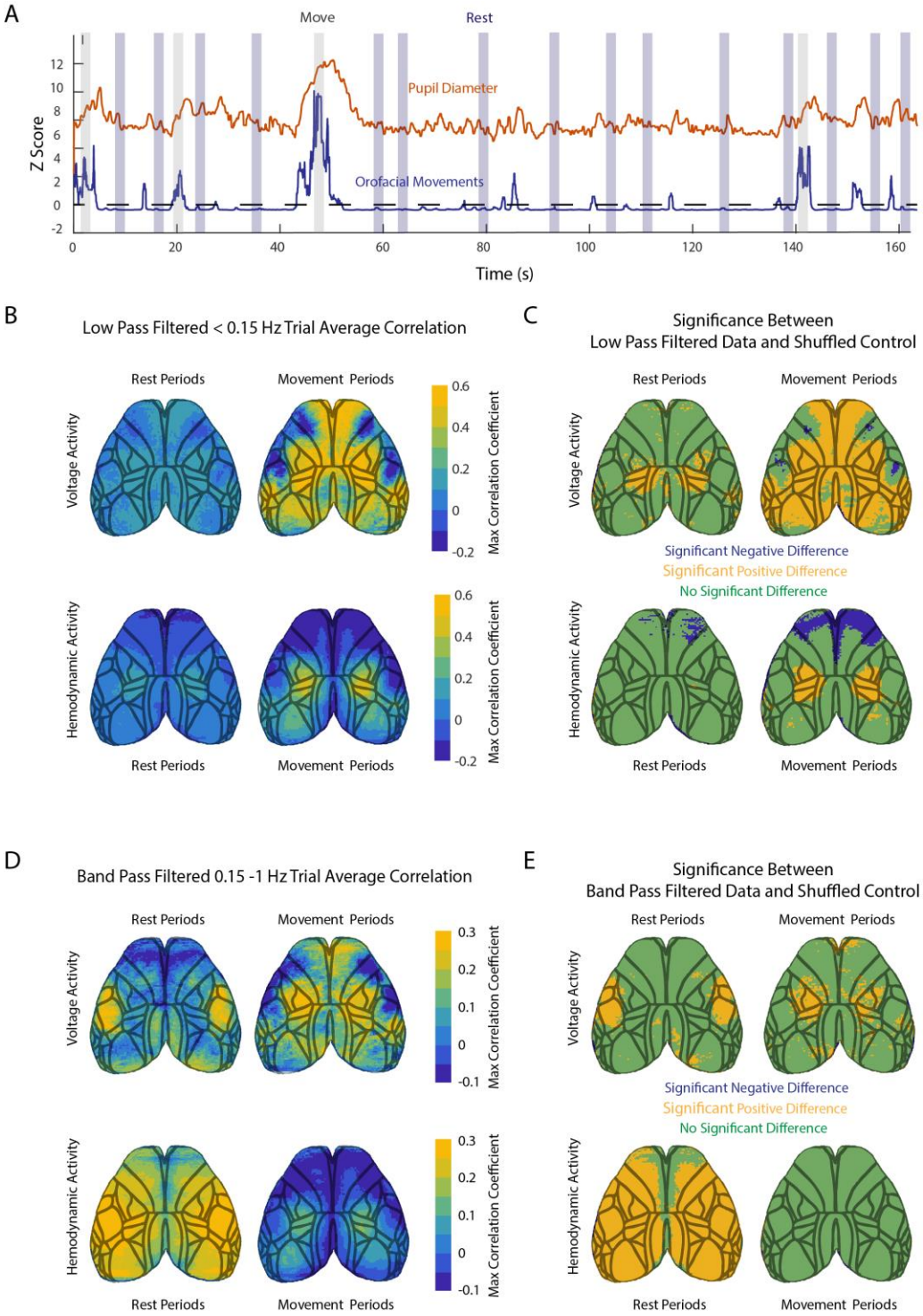

Figure 5 **Patterns of cortical coupling to pupil diameter are dependent on behavioral state A.** Example trial showing pupil diameter (red) and orofacial movement (green). Movement periods (shaded gray) were classified based on the movement signal remaining above the threshold (dashed line) for at least 2s. Periods of rest were instead identified when the movement signal remained below the threshold for at least 2 seconds. **B.** Top left shows the average correlation map (n = 65 trials) for cortical voltage activity (lowpass filtered <0.15Hz) and pupil diameter for periods of rest. Top right shows the voltage correlation map during periods of facial movement. The bottom panels show the same analysis for hemodynamic activity. **C.** Statistical map showing significantly different areas between what's displayed in panel B with a shuffled control, adjusted for multiple comparisons. **D.** Same activity and behavior trials as in C but now bandpass filtered (0.15- 1 Hz). **E.** Same statistical significance as shown in panel C but for band pass filtered data in E**.** For panels C and E the areas labeled in blue and yellow represent areas that have a significant negative and positive difference to the control respectively, while green is areas with no significant difference.

Discussion

In this work we characterized the temporal and spatial components of cortical coupling to arousal as measured through changes in pupil diameter. Using wide-field imaging of the voltage sensitive fluorescent protein Butterfly 1.2 we were able to record both membrane voltage and hemodynamic activity bilaterally across a large extent of mouse dorsal cortex. We found that cortical global voltage signal obtained was tightly coupled to pupil diameter. The cortical signals measured here were differentially coupled to pupil diameter across multiple frequencies and distinct functional cortical areas. The observed patterns were also dependent on behavioral state where periods of prolonged orofacial movements had differential effects on the observed voltage and hemodynamic activity.

The voltage sensitive fluorescent protein used is optimized to show the greatest changes in fluorescence in the sub-threshold voltage range (Akemann et al., 2012). This allows us to capture activity changes that are not visible with calcium sensors, which are the more commonly used counterpart to voltage sensors in part due to their better signal to noise ratio. Capturing subthreshold activity is of particular importance when studying the influence of pupil diameter on cortical activity because these changes may be primarily coupled across sub-threshold fluctuations as observed in intracellular recordings (McGinley M., 2015; McGinley et al., 2015).

Cortical networks linking spontaneous fluctuations to changes in arousal

Constant variations in the state of the brain contribute to the apparent noisiness of sensory responses at both the neural and behavioral levels (McGinley et al., 2015). Spontaneous fluctuations in the global brain state are said to encode changes in cognitive variables such as changes in arousal state (Jacobs, Steinmetz, Peters, Carandini, & Harris, 2020; Pisauro et al., 2016). Changes in arousal as measured by pupil diameter are known to be an indicator of locus coeruleus activity which controls the release of norepinephrine (NE) through its expansive projections across the brain (Bekar, Wei, & Nedergaard, 2012; Reimer et al., 2016). Enhanced cortical NE is associated with a decrease in vessel diameter. Such vasocontraction could drive the slight net negative correlation we observe between the two (Bekar et al., 2012). This contrasts with what we observe in the presence of active behavior. In those cases, the vasodilatory signals from local neural activity push the hemodynamic response into being net positive (Turner, Gheres, & Drew, 2022). This can be seen when separating the trials into periods of movement and rest for the infraslow range. The periods of positive correlation between hemodynamics and pupil diameter are driven by those active periods. At rest the spontaneous hemodynamic signal changes reflect a combination of local neural activity and non-neuronal responses (Winder, Echagarruga, Zhang, & Drew, 2017).

While the global signal is often considered a nuisance variable in fMRI imaging, we found that the global signal for voltage activity was tightly coupled throughout cortex to changes in arousal as measured by pupil diameter (Fox et al., 2008; Macey, Macey, Kumar, & Harper, 2003). Furthermore, our results show that arousal influences distinct cortical regions for both voltage and hemodynamic activity. For both signals there is a positive correlation between medial sensory-motor cortices as well as more laterally in the secondary sensory/auditory cortices. Additionally, arousal also influenced frontal motor/cognitive cortical areas that were negatively correlated with arousal. Thus, removal of global signal during pre-processing should be carefully considered because its influence is spatially variant and serves as a covariate for changes in arousal or attention(Xu et al., 2018).

The largest network difference between the voltage and hemodynamic signals, when related to changes in arousal, is observed in the pre-frontal cortex. Voltage activity in pre-frontal cortex is positively correlated with arousal while there is a net negative correlation observed in these same areas for hemodynamic activity. Pre-frontal cortex plays a large role in the default mode network (DMN), a rsfMRI network that emerges as an anatomically distributed set of brain regions with low-frequency correlated activity in the absence of a goal-directed task (Raichle, 2015). Over 70% of the DMN areas in the mouse reside in the isocortex consisting of prefrontal, medial and somatosensory areas (Whitesell et al., 2021). Notably our results highlight the possibility that arousal has differential influences on pre-frontal cortex during resting state for hemodynamics and voltage activity. This can have subsequent implications for how resting state networks are identified and interpreted.

Temporal profiles of resting state signals

The spectral decomposition of our observed arousal signals fluctuates across both fast and slow timescales. We found that arousal changes as reflected by fluctuations in pupil diameter were differentially coupled to voltage and hemodynamic activity across distinct frequencies. The spectral decomposition revealed the strong coupling between pupil with voltage and hemodynamic activity up to 0.2 Hz. The slow fluctuations on the order of seconds that were observed in both voltage and hemodynamic activity therefore track the slow fluctuations in arousal (Reimer et al., 2014). Distinct time courses for each frequency band could represent state fluctuations between periods of low and high arousal. Low arousal represented by pupil constriction was characterized by an increased low-frequency oscillations and higher ensemble correlations (Chan, Mohajerani, LeDue, Wang, & Murphy, 2015; Reimer et al., 2014). Pupil dilation, representing an increase in arousal and a subsequent increase in locomotion results in a suppression of a low frequency (<4Hz) band (McGinley et al., 2015).

Inconsistencies in the time scale of slow hemodynamics and well-recognized faster neuronal oscillations that are observed with electrophysiology make it challenging to establish a direct relationship between the two. We show here that the infraslow and slow frequency components of both the voltage and hemodynamic signals exhibited a direct relationship to changes in arousal and to each other. This is particularly relevant for BOLD-fMRI which typically cannot capture frequencies > 0.5 -1 Hz due to limitations of the imaging system and inherent low-pass filter properties of the vasculature (Kim, Richter, & Uğurbil, 1997). Band-limited LFP is known to correlate to BOLD, but infraslow LFP waves have also been shown to be compatible in time scale with the slow BOLD fluctuations that occur in spontaneous activity making them ideal candidates for the neural basis of the BOLD signal and for coordinating activity between large-scale brain regions (Pan, Thompson, Magnuson, Jaeger, & Keilholz, 2013). Neuroimaging advances measuring in vivo at both high temporal and spatial resolution hold a lot of promise for probing this relationship across different scales (Lewis, Setsompop, Rosen, & Polimeni, 2016; Toi et al., 2022).

Patterns of cortical coupling to pupil diameter are dependent on behavioral state

Expanding on initial attempts to link arousal related to voltage activity across cortex for periods of locomotion, we demonstrate that pupil dynamics were coupled to neural activity also in the absence of locomotion (Shimaoka et al., 2018; Vinck et al., 2015). Our work describes the behavioral-dependent remapping of distributed cortical networks in spontaneously behaving mice. While there is no locomotion in our experiments, these head-fixed mice do undergo periods of complete stillness/rest and periods of prolonged uninstructed orofacial movements. Such orofacial movements have been shown with wide-field calcium imaging to be associated with strong neural activity changes over complex cortical networks (Musall, Kaufman, Juavinett, Gluf, & Churchland, 2019). We find that similar to

locomotion orofacial movement is associated with periods of arousal indicated by increased pupil diameter (Fig. 5A). Changes in arousal indicated by locomotion are known to lead to increased neural activity in motor areas, retrosplenial cortex and sensory cortices (Clancy, Orsolic, & Mrsic-Flogel, 2019). We found that in a similar manner periods of uninstructed orofacial movements resulted in increases in correlation between voltage and pupil in medial sensory-motor areas and decreased correlations in lateral motor and sensory areas.

A previous study employed cerebral blood volume (CBV) imaging and electrophysiological local field potential and multi-unit activity recordings in relation to locomotion(Huo, Smith, & Drew, 2014). This study showed that pre-frontal cortex and other nonprimary sensory areas have a decreased hemodynamic signal as measured by CBV associated with voluntarily locomotion. In fMRI this is interpreted as a decrease in neural activity in these areas (Buckner, Andrews-Hanna, & Schacter, 2008; Fox et al., 2008). However, the electrophysiological measurements by Huo et al. showed that multiunit activity increased in frontal cortical areas during locomotion. Our voltage imaging results complement this finding by a similar dissociation between our hemodynamic signal and our voltage activity map in prefrontal cortex. In addition, we determined that this effect was due to changes in infraslow frequency correlations between pupil diameter and hemodynamics, and an opposite effect was seen in the S1/M1 areas.

A mechanistic understanding of how fMRI recording of resting-state activity is influenced by arousal is critical both for the interpretation of future resting-state data and for understanding how cortical states influence behavior and functional network configurations. Our results highlight that functional networks determined with hemodynamic measurements only partially overlap with voltage activity networks with respect to arousal. We found that functional networks related to different behavioral states are modulated by arousal differently. Further, we found that different signal frequency bands revealed different functional networks and differed in their relation to brain voltage activity. Therefore, arousal related effects on fMRI should be carefully considered when interpreting functional networks related to brain activity. Future work should carefully delineate the influence on cholinergic and adrenergic signals that control arousal on hemodynamic signaling. Studies to date suggest a significant spatial and temporal heterogeneity in this regard (DiNuzzo et al., 2019; Lohani et al., 2021; Schneider et al., 2016; Winder et al., 2017).

Bibliography

Akemann, W., Mutoh, H., Perron, A., Park, Y. K., Iwamoto, Y., & Knopfel, T. (2012). Imaging neural circuit dynamics with a voltage-sensitive fluorescent protein. *J Neurophysiol, 108*(8), 2323-2337. doi:10.1152/jn.00452.2012

Alnaes, D., Sneve, M. H., Espeseth, T., Endestad, T., de Pavert, S., & Laeng, B. (2014). Pupil size signals mental effort deployed during multiple object tracking and predicts brain activity in the dorsal attention network and the locus coeruleus. *Journal of Vision, 14*(4). doi:10.1167/14.4.1

Bekar, L. K., Wei, H. S., & Nedergaard, M. (2012). The Locus Coeruleus-Norepinephrine Network Optimizes Coupling of Cerebral Blood Volume with Oxygen Demand. *Journal of Cerebral Blood Flow & Metabolism, 32*(12), 2135-2145. doi:10.1038/jcbfm.2012.115

Biswal, B., Zerrin Yetkin, F., Haughton, V. M., & Hyde, J. S. (1995). Functional connectivity in the motor cortex of resting human brain using echo-planar mri. *Magnetic Resonance in Medicine, 34*(4), 537-541. doi:https://doi.org/10.1002/mrm.1910340409

Breeden, A. L., Siegle, G. J., Norr, M. E., Gordon, E. M., & Vaidya, C. J. (2017). Coupling between spontaneous pupillary fluctuations and brain activity relates to inattentiveness. *European Journal of Neuroscience, 45*(2), 260-266. doi:https://doi.org/10.1111/ejn.13424

Buckner, R. L., Andrews-Hanna, J. R., & Schacter, D. L. (2008). The Brain's Default Network. *Annals of the New York Academy of Sciences, 1124*(1), 1-38. doi:https://doi.org/10.1196/annals.1440.011

Carandini, M., Shimaoka, D., Rossi, L. F., Sato, T. K., Benucci, A., & Knopfel, X. (2015). Imaging the awake visual cortex with a genetically encoded voltage indicator. *Journal of Neuroscience, 35*(1), 53-63. Retrieved from http://www.scopus.com/inward/record.url?eid=2-s2.0-84920540758&partnerID=40&md5=dd180abac0429fd141cf61162a147c6c

Chan, A. W., Mohajerani, M. H., LeDue, J. M., Wang, Y. T., & Murphy, T. H. (2015). Mesoscale infraslow spontaneous membrane potential fluctuations recapitulate high-frequency activity cortical motifs. *Nat Commun, 6*, 7738. doi:10.1038/ncomms8738

Clancy, K. B., Orsolic, I., & Mrsic-Flogel, T. D. (2019). Locomotion-dependent remapping of distributed cortical networks. *Nat Neurosci, 22*(5), 778-786. doi:10.1038/s41593-019-0357-8

DiNuzzo, M., Mascali, D., Moraschi, M., Bussu, G., Maugeri, L., Mangini, F., . . . Giove, F. (2019). Brain Networks Underlying Eye's Pupil Dynamics. *Frontiers in Neuroscience, 13*. Retrieved from https://www.frontiersin.org/articles/10.3389/fnins.2019.00965

Ferezou, I., Haiss, F., Gentet, L. J., Aronoff, R., Weber, B., & Petersen, C. C. (2007). Spatiotemporal dynamics of cortical sensorimotor integration in behaving mice. *Neuron, 56*(5), 907-923. doi:10.1016/j.neuron.2007.10.007

Fox, M. D., Zhang, D., Snyder, A. Z., & Raichle, M. E. (2008). The Global Signal and Observed Anticorrelated Resting State Brain Networks.

Huo, B.-X., Smith, J. B., & Drew, P. J. (2014). Neurovascular Coupling and Decoupling in the Cortex during Voluntary Locomotion. *Journal of Neuroscience*.

Jacobs, E. A. K., Steinmetz, N. A., Peters, A. J., Carandini, M., & Harris, K. D. (2020). Cortical State Fluctuations during Sensory Decision Making. *Curr Biol, 30*(24), 4944-4955 e4947. doi:10.1016/j.cub.2020.09.067

Kim, S.-G., Richter, W., & Uğurbil, K. (1997). Limitations of temporal resolution in functional MRI. *Magnetic Resonance in Medicine, 37*(4), 631-636. doi:https://doi.org/10.1002/mrm.1910370427

Lewis, L. D., Setsompop, K., Rosen, B. R., & Polimeni, J. R. (2016). Fast fMRI can detect oscillatory neural activity in humans. *Proceedings of the National Academy of Sciences, 113*(43), E6679-E6685. doi:10.1073/pnas.1608117113

Lohani, S., Moberly, A. H., Benisty, H., Landa, B., Jing, M., Li, Y., . . . Cardin, J. A. (2021). Dual color mesoscopic imaging reveals spatiotemporally heterogeneous coordination of cholinergic and neocortical activity. *bioRxiv*, 2020.2012.2009.418632. doi:10.1101/2020.12.09.418632

Ma, Y., Shaik, M. A., Kim, S. H., Kozberg, M. G., Thibodeaux, D. N., Zhao, H. T., . . . Hillman, E. M. C. (2016). Wide-field optical mapping of neural activity and brain haemodynamics: considerations and novel approaches. *Philosophical Transactions of the Royal Society B: Biological Sciences, 371*(1705), 20150360. doi:10.1098/rstb.2015.0360

Macey, P. M., Macey, K. E., Kumar, R., & Harper, R. M. (2003). A method for removal of global effects from fMRI time series.

Madisen, L., Garner, Aleena R., Shimaoka, D., Chuong, Amy S., Klapoetke, Nathan C., Li, L., . . . Zeng, H. (2015). Transgenic Mice for Intersectional Targeting of Neural Sensors and Effectors with High Specificity and Performance. *Neuron, 85*(5), 942-958. doi:https://doi.org/10.1016/j.neuron.2015.02.022

McGinley M., D. S., McCormick D. (2015). Cortical Membrane Potential Signature of Optimal States for Sensory Signal Detection. *Neuron*.

McGinley, M. J., Vinck, M., Reimer, J., Batista-Brito, R., Zagha, E., Cadwell, C. R., . . . McCormick, D. A. (2015). Waking State: Rapid Variations Modulate Neural and Behavioral Responses. *Neuron, 87*(6), 1143-1161. doi:10.1016/j.neuron.2015.09.012

Meyer-Baese, L., Watters, H., & Keilholz, S. (2022). Spatiotemporal patterns of spontaneous brain activity: a mini-review. *Neurophotonics, 9*(3), 032209. doi:10.1117/1.NPh.9.3.032209

Murphy, P. R., O'Connell, R. G., O'Sullivan, M., Robertson, I. H., & Balsters, J. H. (2014). Pupil Diameter Covaries With BOLD Activity in Human Locus Coeruleus. *Human Brain Mapping, 35*(8), 4140-4154. doi:10.1002/hbm.22466

Musall, S., Kaufman, M., Juavinett, A., Gluf, S., & Churchland, A. (2019). Single-trial neural dynamics are dominated by richly varied movements.

Pais-Roldán, P., Mateo, C., Pan, W.-J., Acland, B., Kleinfeld, D., Snyder, L. H., . . . Keilholz, S. (2021). Contribution of animal models toward understanding resting state functional connectivity. *Neuroimage, 245*, 118630. doi:https://doi.org/10.1016/j.neuroimage.2021.118630

Pan, W. J., Thompson, G. J., Magnuson, M. E., Jaeger, D., & Keilholz, S. (2013). Infraslow LFP correlates to resting-state fMRI BOLD signals. *Neuroimage, 74*, 288-297. doi:10.1016/j.neuroimage.2013.02.035

Pisauro, M. A., Benucci, A., & Carandini, M. (2016). Local and global contributions to hemodynamic activity in mouse cortex. *J Neurophysiol, 115*(6), 2931-2936. doi:10.1152/jn.00125.2016

Poulet, J. F. A., & Petersen, C. C. H. (2008). Internal brain state regulates membrane potential synchrony in barrel cortex of behaving mice. *Nature, 454*(7206), 881-885. doi:10.1038/nature07150

Raichle, M. E. (2015). The Brain's Default Mode Network. *Annual Review of Neuroscience, 38*(1), 433-447. doi:10.1146/annurev-neuro-071013-014030

Ratzlaff, E. H., & Grinvald, A. (1991). A tandem-lens epifluorescence macroscope: Hundred-fold brightness advantage for wide-field imaging. *Journal of Neuroscience Methods, 36*(2), 127-137. doi:https://doi.org/10.1016/0165-0270(91)90038-2

Reimer, J., Froudarakis, E., Cadwell, C. R., Yatsenko, D., Denfield, G. H., & Tolias, A. S. (2014). Pupil fluctuations track fast switching of cortical states during quiet wakefulness. *Neuron, 84*(2), 355-362. doi:10.1016/j.neuron.2014.09.033

Reimer, J., McGinley, M. J., Liu, Y., Rodenkirch, C., Wang, Q., McCormick, D. A., & Tolias, A. S. (2016). Pupil fluctuations track rapid changes in adrenergic and cholinergic activity in cortex. *Nat Commun, 7*, 13289. doi:10.1038/ncomms13289

Schneider, M., Hathway, P., Leuchs, L., Samann, P. G., Czisch, M., & Spoormaker, V. I. (2016). Spontaneous pupil dilations during the resting state are associated with activation of the salience network. *Neuroimage, 139*, 189-201. doi:10.1016/j.neuroimage.2016.06.011

Shimaoka, D., Harris, K. D., & Carandini, M. (2018). Effects of Arousal on Mouse Sensory Cortex Depend on Modality. *Cell Rep, 22*(12), 3160-3167. doi:10.1016/j.celrep.2018.02.092

Silasi, G., Xiao, D., Vanni, M. P., Chen, A. C. N., & Murphy, T. H. (2016). Intact skull chronic windows for mesoscopic wide-field imaging in awake mice. *Journal of Neuroscience Methods, 267*, 141-149. doi:https://doi.org/10.1016/j.jneumeth.2016.04.012

Stringer, C., Pachitariu, M., Steinmetz, N., Reddy, C. B., Carandini, M., & Harris, K. D. (2019). Spontaneous behaviors drive multidimensional, brainwide activity. *Science, 364*(6437), 255. doi:10.1126/science.aav7893

Toi, P. T., Jang, H. J., Min, K., Kim, S.-P., Lee, S.-K., Lee, J., . . . Park, J.-Y. (2022). In vivo direct imaging of neuronal activity at high temporospatial resolution. *Science, 378*(6616), 160-168. doi:10.1126/science.abh4340

Turner, K. L., Gheres, K. W., & Drew, P. J. (2022). Arousal state dependence of the cortical blood volume – pupil diameter relationship. *bioRxiv*, 2022.2006.2015.496309. doi:10.1101/2022.06.15.496309

Turner, K. L., Gheres, K. W., Proctor, E. A., & Drew, P. J. (2020). Neurovascular coupling and bilateral connectivity during NREM and REM sleep. *Elife, 9*, e62071. doi:10.7554/eLife.62071

Vinck, M., Batista-Brito, R., Knoblich, U., & Cardin, J. A. (2015). Arousal and locomotion make distinct contributions to cortical activity patterns and visual encoding. *Neuron, 86*(3), 740-754. doi:10.1016/j.neuron.2015.03.028

Whitesell, J. D., Liska, A., Coletta, L., Mihalas, S., Gozzi, A., & Harris, J. A. (2021). Regional, Layer, and Cell-Type-Specific Connectivity of the Mouse Default Mode Network. *Neuron*.

Winder, A. T., Echagarruga, C., Zhang, Q., & Drew, P. J. (2017). Weak correlations between hemodynamic signals and ongoing neural activity during the resting state. *nature neuroscience, 20*(12), 1761-1769. doi:10.1038/s41593-017-0007-y

Xu, H., Su, J., Qin, J., Li, M., Zeng, L.-L., Hu, D., & Shen, H. (2018). Impact of global signal regression on characterizing dynamic functional connectivity and brain states. *Neuroimage, 173*, 127-145. doi:https://doi.org/10.1016/j.neuroimage.2018.02.036